Journal of Materials Chemistry C

ROYAL SOCIETY OF CHEMISTRY

PAPER

View Article Online
View Journal | View Issue



Cite this: J. Mater. Chem. C, 2023, 11, 11905

# Dithiene-fused quinoxalineimide-based all-acceptor polymers for n-type organic semiconductors†

Lijun Tu,[a] Hao Wang,[a] Xiangya Li,[a] Xin Wang,[a] Mingwei Li,[a] Yang Wang *[b] and Yongqiang Shi*[a]

Received 27th June 2023,
Accepted 5th July 2023

DOI: 10.1039/d3tc02243a

rsc.li/materials-c

Introduction of strong electron-deficient building blocks into the polymer backbone is an efficient strategy to design n-type organic semiconductors. In this work, a strong electron-deficient building block, dithiene-fused quinoxalineimide (DTQI), containing electron-withdrawing quinoxaline and imide units, was synthesized and incorporated into a polymer backbone. The frontier molecular orbital (FMO) energy levels downshifted with the incorporation of the quinoxalineimide (QI) unit onto the framework. Owing to the high electron-affinity of DTQI, the DTQI-based acceptor–acceptor (all-acceptor, A–A) type polymer P(DTQI-BTI) showed deep-lying highest occupied molecular orbital (HOMO) and lowest unoccupied molecular orbital (LUMO) energy levels, thus yielding unipolar n-type transport character with electron mobility of 0.25 $cm^2 V^{-1} s^{-1}$ in organic thin-film transistors. These results demonstrate that DTQI is a promising building block for constructing n-type polymer semiconductors and can be extended to the design of other novel electron-deficient building blocks.



[a] Key Laboratory of Functional Molecular Solids, Ministry of Education, and School of Chemistry and Materials Science, Anhui Normal University, Wuhu, Anhui 241002, China. E-mail: shiyq@ahnu.edu.cn
[b] Laboratory of Molecular Materials and Devices, State Key Laboratory of Molecular Engineering of Polymers, Department of Materials Science, Fudan University, 2005, Songhu Road, Shanghai 200438, P. R. China. E-mail: yangwang@fudan.edu.cn

† Electronic supplementary information (ESI) available. See DOI: https://doi.org/10.1039/d3tc02243a

Yongqiang Shi

*Yongqiang Shi is a Professor at School of Chemistry and Materials Science, Anhui Normal University. Before that, he carried out research as a research assistant at Southern University of Science and Technology in 2015–2020 under the supervision of Prof. Xugang Guo. He received his PhD degree from Southwest Petroleum University in 2020. He worked as a "Hong Kong Scholars Program" postdoctoral fellow in the group of Prof. Qichun Zhang at City University of Hong Kong. His research focuses on the design and synthesis of n-type polymers for organic thin-film transistors, polymer solar cells, perovskite solar cells, and organic thermoelectrics.*

## Introduction

n-Type organic semiconductors are an excellent important class of active materials in organic optoelectronic devices, such as organic thin-film transistors (OTFTs),[1–13] organic photovoltaics (OPVs),[14–18] perovskite solar cells (PVSCs),[19–21] and organic thermoelectrics (OTEs).[22–29] In the past few decades, tremendous efforts have been made to develop p-type (hole transport) and ambipolar (both hole and electron transport) semiconducting polymers.[30–34] However, the development of n-type (electron transport) polymer semiconductors lags behind their p-type counterparts due to the limited electron-deficient building blocks.[35–37] To realize practical organic electron devices, both n-type and p-type organic semiconductors are required. Therefore, it is necessary and urgent to design and synthesize n-type polymer semiconductors.

To realize unipolar n-type electron transport in polymer semiconductors, both the highest occupied molecular orbital (HOMO) and lowest unoccupied molecular orbital (LUMO) energy levels should be sufficiently low. One of the efficient strategies to design n-type polymer semiconductors is to introduce strong electron-deficient building blocks into the backbone, such as imide,[38–42] amide,[4,43–46] cyano,[47] or B ← N groups.[48–52] Among them, imide functionalization has become one of the widely investigated acceptor building blocks for constructing n-type organic semiconductors, which exhibits intriguing optoelectronic properties due to the strong

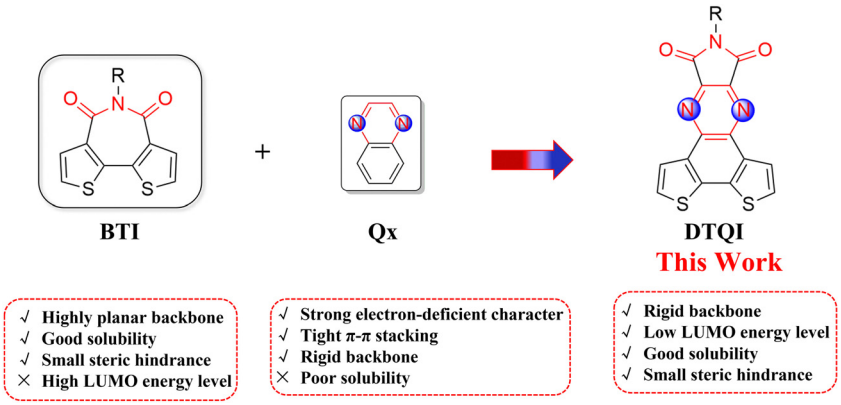


Fig. 1 Molecular design strategy to develop electron-deficient building block DTQI, which combines the advantages of both BTI and Qx.



electron-withdrawing character of the imide group and good solubility enabled by the *N*-alkyl side chain. As typical representatives of imide building blocks, naphthalene diimide (NDI),[1,53] perylene diimide (PDI),[8,54,55] naphthodithiophene diimide (NDTI),[56,57] dithienophtalimide (DTP),[58,59] and bithiophene imide (BTI),[5] have been widely incorporated into n-type polymer semiconductors. NDI and PDI containing diimide groups are beneficial to realizing the low-lying LUMO energy levels. However, the geometries of NDI and PDI result in sizable steric hindrance with neighboring units and lead to a distorted polymer backbone, which limits electron transport. Recently, BTI (Fig. 1) has shown remarkable success in developing high-performance n-type polymer semiconductors and the BTI-based A–A type polymers have yielded promising device performance in OTFTs, PVSCs, and OTEs.[19,23,35]

Among various acceptor units, a pyrazine-fused electron-deficient unit is also a promising building block to construct n-type polymer semiconductors due to its strong electron-withdrawing ability, easy functionalization, and tunable LUMO levels.[60,61] For example, pyrazine derivatives, such as quinoxaline (Qx) (Fig. 1), fluorinated quinoxaline, thiadiazoloquinoxaline, and dithienobenzoquinoxaline, have been widely developed as high mobility semiconductors for OTFTs.[62,63] By proper modification of pyrazine-based acceptor units, the energy levels and charge carrier mobility can be easily tuned by the following methods: (i) changing the quinoxaline-based polymer backbone from acceptor–donor to acceptor–acceptor; (ii) introduction of different side chains to tune the solubility, aggregation behavior and intermolecular interactions of the molecule, which in turn affects the device performance of the polymer; (iii) introduction of functional groups onto the quinoxaline backbones, such as F atoms, Cl atoms, and cyano and ester groups, to lower the LUMO energy levels of the polymers. Therefore, it is highly desired to design other novel pyrazine-based acceptor units and investigate their structure–property relationship.

Inspired by the excellent performance of both BTI- and pyrazine-based organic semiconductors, herein, a dithiene fused quinoxalineimide (DTQI) (Fig. 1) electron-deficient building block, containing electron-withdrawing quinoxaline and imide units, was synthesized and incorporated into polymer semiconductors. DTQI-based A–A type polymers PDTQI and P(DTQI-BTI) exhibit a highly planar backbone and low LUMO energy levels. The low-lying LUMOs ($<-3.50$ eV) of the polymers could effectively facilitate electron injection in OTFTs. P(DTQI-BTI) showed a high $\mu_e$ of $>0.25$ cm$^2$ V$^{-1}$ s$^{-1}$. The results demonstrate that dithiene-fused quinoxalineimide is a promising electron-deficient building block for constructing n-type polymer semiconductors.

## Results and discussion

### Materials synthesis and characterization

The synthetic route to monomer DTQI and its corresponding A–A type polymers PDTQI and P(DTQI-BTI) is depicted in Scheme 1, and the detailed synthetic procedures are provided in the ESI.† Compound **1** was synthesized according to the reported procedure.[64,65] Key intermediate compound **2** was obtained *via* the condensation of **1** with diethyl 2,3-dioxosuccinate. **2** was then dibrominated with NBS to yield **3**. Carboxylic acid compound **4** was obtained by hydrolysis with sodium hydroxide and successive hydrochloric acid treatment, and then **4** was treated with acetyl chloride to yield acid anhydride **5**. The imide molecule DTQI-2Br was successfully obtained by amidation of compound **5** with the corresponding alkylamine and successive imidization by using acetic anhydride. The monomer and key intermediates were fully characterized by $^1$H NMR and $^{13}$C NMR (Fig. S1–S8, ESI†).

The polymerization of DTQI-2Br was carried out with comonomers bis(tributyltin) and distannylated BTI (BTI-Tin) *via* the Stille coupling reaction using $Pd_2(dba)_3$/P(*o*-tol)$_3$ as the catalyst system to afford A–A type polymers PDTQI and P(DTQI-BTI), respectively (Scheme 1b). BTI-Tin was chosen as the comonomer due to its high planar backbone, good solubility and high reactivity.[12] Additionally, incorporation of BTI into the polymer backbone would increase the content of acceptor unit and allow us to tune the frontier molecular orbital levels of the conjugated polymers. After polymerization, the polymers were purified by successive Soxhlet extractions with methanol, acetone,

 

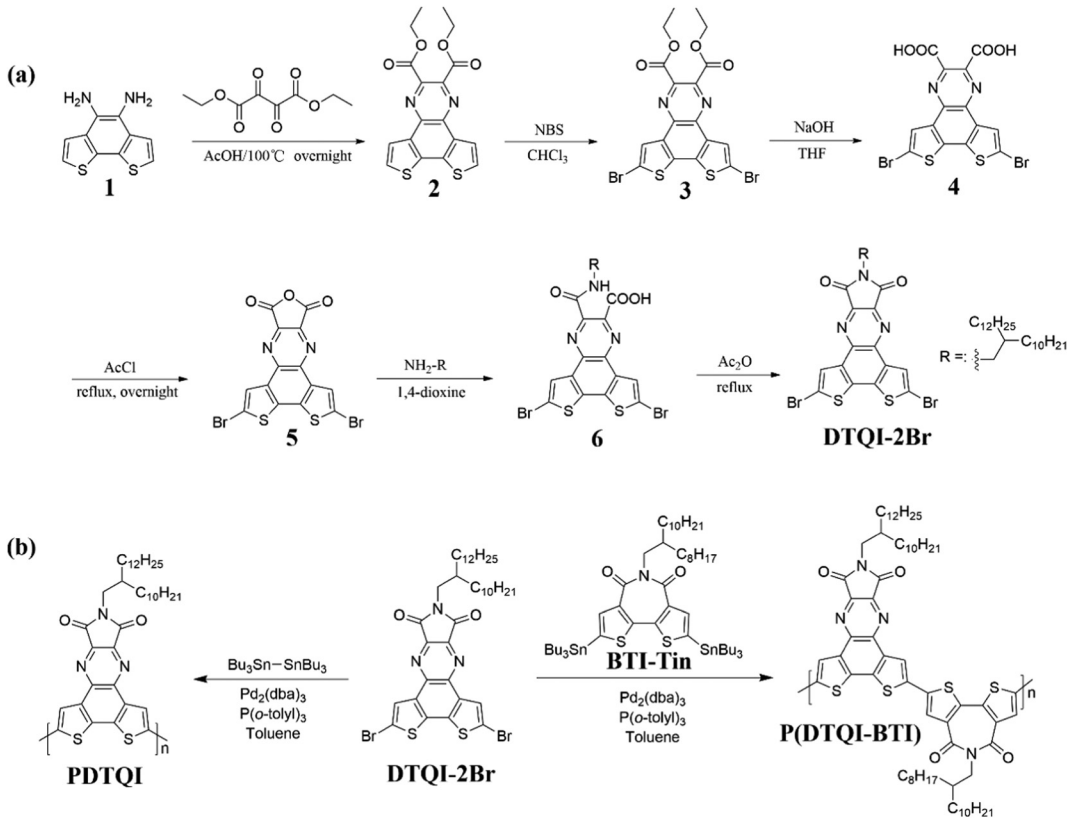


Scheme 1 Synthetic route to (a) the dibrominated dithiene-fused quinoxalineimide monomer DTQI-2Br and (b) DTQI-based A–A type polymers PDTQI and P(DTQI-BTI).

hexane, dichloromethane and chloroform. The final chloroform fractions were collected and reprecipitated into methanol to afford the A–A type polymers, which were used for characterization and device fabrication. The number-average molecular weights ($M_n$s) of the polymers were measured by high-temperature gel permeation chromatography (HT-GPC) with 1,2,4-trichlorobenzene as the eluent at 150 °C. As summarized in Table 1, PDTQI has an $M_n$ of 54 kDa with a polydispersity index (PDI) of 1.8, and P(DTQI-BTI) shows an $M_n$ of 65 kDa with a PDI of 1.7.

## Polymer thermal properties

The thermal properties of the two A–A type polymers were investigated by thermogravimetric analysis (TGA) and differential scanning calorimetry (DSC). As shown in Fig. S9 (ESI†), both polymers exhibited excellent thermal stability with the decomposition temperature (5% weight loss) over 400 °C. DSC shows clearly distinct thermal properties of PDTQI, and a glass transition temperature ($T_g$) of 153 °C was detected during the heating scan. The exothermic peak at ≈250 °C corresponded to the phase transition temperature of PDTQI, while for P(DTQI-BTI), no endothermic or exothermic peak was observed during the heating or cooling process, revealing that no phase transitions were observed within the temperature range (25–350 °C).

## Theoretical calculations

To evaluate the electronic structure and optimized geometry of DTQI, density functional theory (DFT) calculations were performed at the B3LYP/6-31G(d) level using the Gaussian 09 program. The optimized molecular geometry of DTQI is a completely planar structure (Fig. S10, ESI†). Compared with BTI, the new DTQI shows a low-lying FMO energy level, which should facilitate electron injection and block hole accumulation, thus resulting in n-type transport character. In

Table 1 Molecular weights, and optical and electrochemical properties of the polymers

| Polymer | $M_n$[a] (KDa) | PDI | $\lambda_{max}^{film}$[b] (nm) | $\lambda_{onset}^{film}$ (nm) | $E_g^{opt}$[c] (eV) | $E_{LUMO}$[d] (eV) | $E_{HOMO}$[e] (eV) |
|---|---|---|---|---|---|---|---|
| PDTQI | 54 | 1.8 | 345 | 627 | 1.98 | −3.60 | −5.58 |
| P(DTQI-BTI) | 65 | 1.7 | 586 | 627 | 1.98 | −3.63 | −5.61 |

[a] GPC *versus* polystyrene standard, trichlorobenzene as the eluent at 150 °C. [b] Absorption of the as-cast film in chloroform solution. [c] Estimated from the absorption onset of the as-cast polymer film using the equation: $E_g^{opt} = 1240/\lambda_{onset}$ (eV). [d] $E_{LUMO} = -e(E_{red}^{onset} + 4.80)$ eV, $E_{red}^{onset}$ determined using the $Fc/Fc^+$ external standard. [e] $E_{HOMO} = E_{LUMO} - E_g^{opt}$.

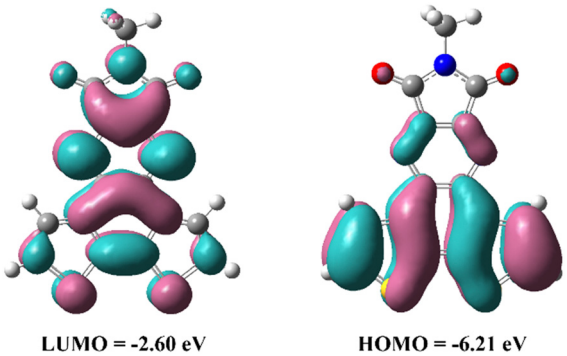


Fig. 2 Frontier molecular orbital energy levels of DTQI.

comparison with BTzI,[33] fusing a bithiophene unit into the quinoxalineimide core can improve the reaction activity between the DTQI monomer and other acceptor comonomers, thus obtaining a polymer with high $M_n$. Therefore, a DTQI building block is favorable for constructing high-performance n-type polymer semiconductors. The $\pi$-electron density distributions of the LUMO levels are widely delocalized over the $\pi$-framework, while the HOMO level is mostly localized around the central phenyl ring and thiophene rings of the DTQI core (Fig. 2). The calculated HOMO and LUMO levels are −6.21 and −2.60 eV for DTQI. The LUMO level of the DTQI is 0.3 eV lower than the calculated LUMO level of the BTI. The relatively lower LUMO level of the DTQI is beneficial for the electron transport. These results confirm that integrating electron-deficient BTI and quinoxaline units into a new building block is an effective strategy for achieving polymer semiconductors with high planar backbones and deep-lying LUMO levels.

### Optical and electrochemical properties

The optical and electrochemical properties of DTQI-based polymers have been evaluated by UV-via absorption spectra and cyclic voltammetry (CV), and the corresponding data are summarized in Table 1. As shown in Fig. 3a, homopolymer PDTQI showed nearly the same absorption spectra in both film and solution. However, P(DTQI-BTI) exhibited two main peaks at 500–600 nm (Fig. 3b), and the long wavelength absorption band of P(DTQI-BTI) is ascribed to the intramolecular charge transfer (ICT). By incorporating a BTI acceptor unit into the P(DTQI-BTI) backbone, the maximum absorption peak of P(DTQI-BTI) is larger than that of PDTQI, suggesting the stronger $\pi$–$\pi$ intermolecular aggregation of P(DTQI-BTI). The optical band gaps ($E_g^{opt}$s) of PDTQI and P(DTQI-BTI) are 1.98 eV, determined from the polymer film absorption onsets.

The electrochemical properties of DTQI-based polymers were evaluated using CV (Fig. 3c). These two polymers exhibit distinctive reduction peaks, indicating their n-type

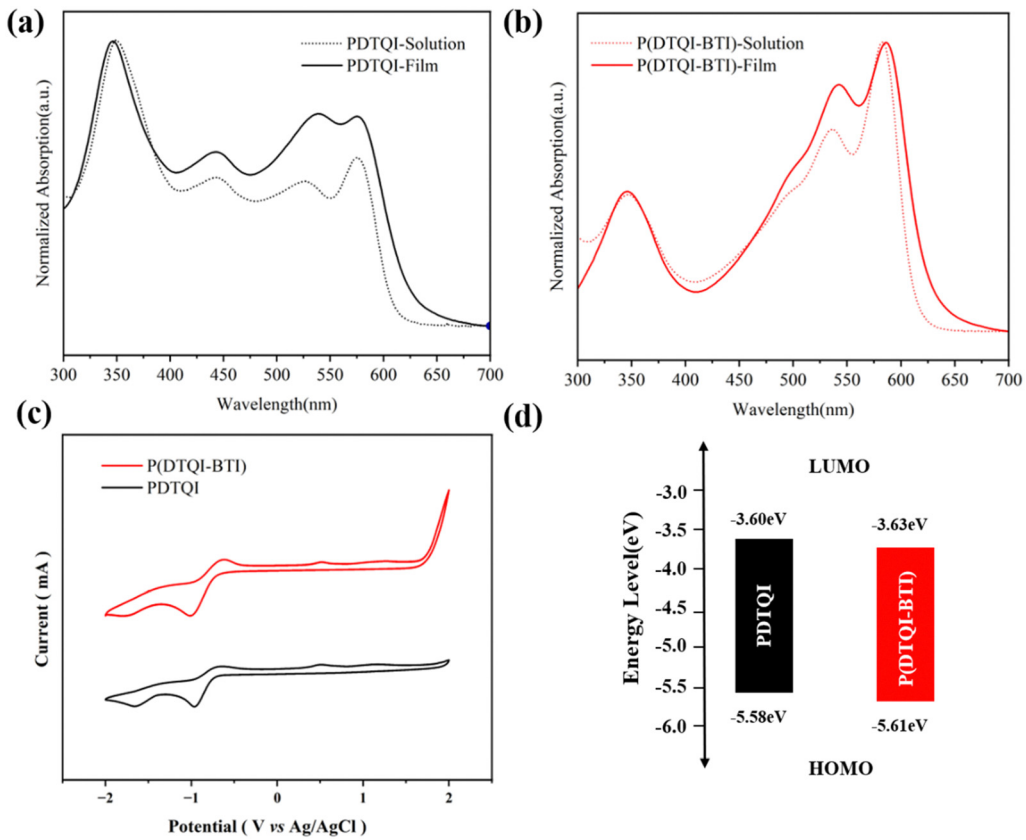


Fig. 3 Normalized UV-vis absorption spectra of the DTQI-based polymers (a) PDTQI and (b) P(DTQI-BTI). (c) Cyclic voltammograms of polymer thin films measured in 0.1 M tetrabutylammonium hexafluorophosphate acetonitrile solution with the $Fc/Fc^+$ redox couple as an external standard at a scanning rate of 0.05 V $s^{-1}$. (d) FMO level diagram of the DTQI-based polymer films.

 

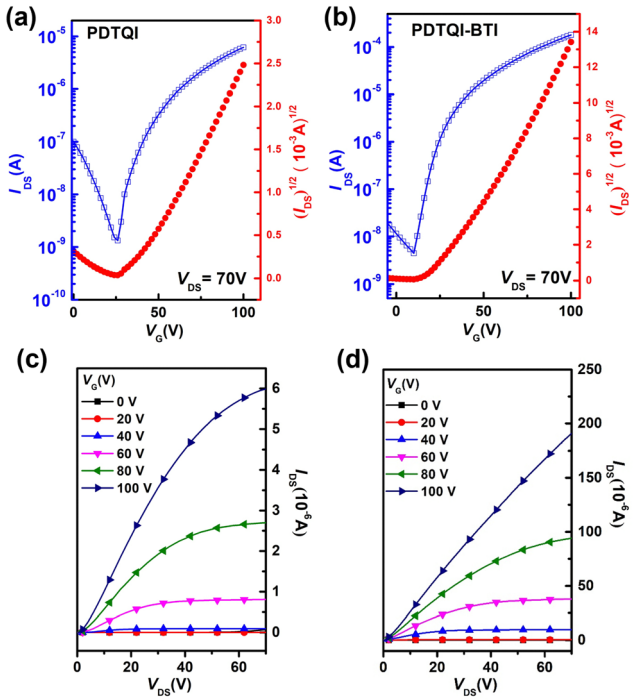


Fig. 4 The transfer (a and b) and output (c and d) curves: (a and c) PDTQI and (b and d) P(DTQI-BTI).

characteristics. According to the onset of reduction potentials, the LUMO energy levels were −3.60 and −3.63 eV for PDTQI and P(DTQI-BTI), respectively. Due to the weak oxidation peaks, the HOMO levels were calculated based on the LUMO and $E_g^{opt}$ using the equation: $E_{HOMO} = E_{LUMO} - E_g^{opt}$, which were −5.58 and −5.61 eV for PDTQI and P(DTQI-BTI), respectively. Therefore, it is found that the DTQI building block containing the electron-withdrawing quinoxaline and imide units, provides the DTQI-based polymers with deep LUMO and HOMO energy levels. Such low-lying FMOs should facilitate electron injection and suppress hole accumulation, thus leading to n-type transport characteristics in OTFTs.

### Charge transport properties of the n-type polymers

To investigate the charge transport properties of PDTQI and P(DTQI-BTI), OTFTs with a top-gate/bottom contact (TGBC) device structure were fabricated. Polymethyl methacrylate (PMMA) is used as the dielectric and Ag is used as the gate electrode. Chloroform is chosen as the processing solvent and the concentration of organic semiconductors is controlled at 5 mg mL$^{-1}$. Before evaluation, an annealing process at 100 °C for 20 min was conducted to achieve better morphology. The

Table 2 The OTFT characteristics based on PDTQI and P(DTQI-BTI)

| Polymers | $\mu_e$ (cm$^2$ V$^{-1}$ s$^{-1}$) | $V_{th}$ (V) | $I_{on}/I_{off}$ ratios |
|---|---|---|---|
| PDTQI | 0.012 (0.01 ± 0.005) | ~30 | ~$10^4$ |
| P(DTQI-BTI) | 0.25 (0.21 ± 0.005) | ~10 | ~$10^5$ |

The average mobility is obtained from 10 devices.

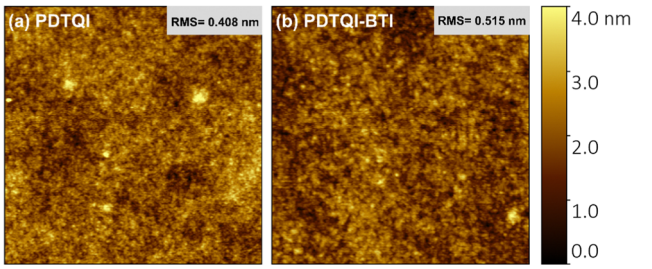


Fig. 5 Tapping-mode AFM topography images of the polymer thin films: (a) PDTQI film and (b) P(DTQI-BTI) film.

saturation mobility of OTFTs is calculated according to the square root of drain current ($I_{DS}$) dependence on gate voltage ($V_G$). The detailed experimental procedures for OTFTs are summarized in the ESI.†Fig. 4a and b show the typical transfer curves and Fig. 4c and d show the corresponding output curves. The related parameters are listed in Table 2. The homopolymer PDTQI exhibits ambipolar charge transport in OTFT. The PDTQI-based device showed $\mu_h$ and $\mu_e$ of 0.005 and 0.012 cm$^2$ V$^{-1}$ s$^{-1}$, respectively, while the copolymer P(DTQI-BTI) showed unipolar n-type charge transport and exhibited one order higher electron mobility of 0.25 cm$^2$ V$^{-1}$ s$^{-1}$ than PDTQI. Besides, a high on/off current ($I_{on}/I_{off}$) ratio of around $10^5$ and a relatively low threshold voltage ($V_{th}$) of 10 V are also achieved by P(DTQI-BTI).

### Film morphology of the n-type polymers

The thin-film morphology of PDTQI and P(DTQI-BTI) is studied by atomic force microscopy (AFM) and the corresponding topography images are shown in Fig. 5. According to the topography images, the PDTQI-based film shows relatively amorphous morphology with the root-mean-square (RMS) roughness value of 0.408 nm. For P(DTQI-BTI), its surfaces are rougher with higher RMS values of 0.515 nm, indicating higher crystallinity.[66,67] As a result, the higher electron mobility of P(DTQI-BTI) might be due to its stronger aggregation of molecules to form films with higher crystallinity. X-Ray diffraction (XRD) analysis was performed to investigate the crystallinity of PDTQI and P(DTQI-BTI) (Fig. S13, ESI†) under the optimal annealing process (100 °C for 20 min).

## Conclusions

In summary, a planar and strong electron-deficient building block, DTQI, containing quinoxaline and imide units has been successfully synthesized and incorporated into a π-conjugated polymer backbone. DTQI combines the advantages of both imide and quinoxaline functionalities, showing a highly planar backbone, good solubility, and small steric hindrance. Due to the strong electron-withdrawing ability of the imide and quinoxaline groups, DTQI has significantly enhanced electron-deficient characteristics. As a consequence, DTQI-based acceptor–acceptor type polymers PDTQI and P(DTQI-BTI) showed deep FMO energy levels, which is beneficial for electron

transport in OTFTs. The resulting OTFT device based on P(DTQI-BTI) shows unipolar n-type behavior with $\mu_e$ of 0.25 $cm^2\ V^{-1}\ s^{-1}$. These results demonstrate that a dithiene-fused quinoxalineimide (DTQI) electron-deficient unit is a promising building block for constructing n-type polymer semiconductors.

## Conflicts of interest

There are no conflicts to declare.

## Acknowledgements

Y. Shi thanks the National Natural Science Foundation of China (No. 22105004).



## References

1 H. Yan, Z. Chen, Y. Zheng, C. Newman, J. R. Quinn, F. Dötz, M. Kastler and A. Facchetti, *Nature*, 2009, **457**, 679–686.
2 Y. Zhao, Y. Guo and Y. Liu, *Adv. Mater.*, 2013, **25**, 5372–5391.
3 C. Zhu, Z. Zhao, H. Chen, L. Zheng, X. Li, J. Chen, Y. Sun, F. Liu, Y. Guo and Y. Liu, *J. Am. Chem. Soc.*, 2017, **139**, 17735–17738.
4 J. Yang, Z. Zhao, S. Wang, Y. Guo and Y. Liu, *Chem*, 2018, **4**, 2748–2785.
5 K. Feng, H. Guo, H. Sun and X. Guo, *Acc. Chem. Res.*, 2021, **54**, 3804–3817.
6 G. Zhang, H. Yu, Y. Sun, W. Wang, Y. Zhao, L. Wang, L. Qiu and Y. Ding, *J. Mater. Chem. C*, 2021, **9**, 633–639.
7 Y. Sui, Y. Shi, Y. Deng, R. Li, J. Bai, Z. Wang, Y. Dang, Y. Han, N. Kirby, L. Ye and Y. Geng, *Macromolecules*, 2020, **53**, 10147–10154.
8 N. Liang, D. Meng and Z. Wang, *Acc. Chem. Res.*, 2021, **54**, 961–975.
9 D. Qu, T. Qi and H. Huang, *J. Energy Chem.*, 2021, **59**, 364–387.
10 W. Yue, M. Nikolka, M. Xiao, A. Sadhanala, C. B. Nielsen, A. J. P. White, H.-Y. Chen, A. Onwubiko, H. Sirringhaus and I. McCulloch, *J. Mater. Chem. C*, 2016, **4**, 9704–9710.
11 D. Patra, J. Lee, S. Dey, J. Lee, A. J. Kalin, A. Putta, Z. Fei, T. McCarthy-Ward, H. S. Bazzi, L. Fang, M. Heeney, M.-H. Yoon and M. Al-Hashimi, *Macromolecules*, 2018, **51**, 6076–6084.
12 H. F. Iqbal, M. Waldrip, H. Chen, I. McCulloch and O. D. Jurchescu, *Adv. Electron. Mater.*, 2021, **7**, 2100393.
13 H. F. Iqbal, Q. Ai, K. J. Thorley, H. Chen, I. McCulloch, C. Risko, J. E. Anthony and O. D. Jurchescu, *Nat. Commun.*, 2021, **12**, 2352.
14 Y. Shi, H. Guo, J. Huang, X. Zhang, Z. Wu, K. Yang, Y. Zhang, K. Feng, H. Y. Woo, R. Ortiz, M. Zhou and X. Guo, *Angew. Chem., Int. Ed.*, 2020, **59**, 14449–14457.
15 G. Wang, F. S. Melkonyan, A. Facchetti and T. J. Marks, *Angew. Chem., Int. Ed.*, 2019, **58**, 4129–4142.
16 Z.-G. Zhang and Y. Li, *Angew. Chem., Int. Ed.*, 2021, **60**, 4422–4433.
17 N. Su, R. Ma, G. Li, T. Liu, L.-W. Feng, C. Lin, J. Chen, J. Song, Y. Xiao, J. Qu, X. Lu, V. K. Sangwan, M. C. Hersam, H. Yan, A. Facchetti and T. J. Marks, *ACS Energy Lett.*, 2021, **6**, 728–738.
18 Y. Shi, R. Ma, X. Wang, T. Liu, Y. Li, S. Fu, K. Yang, Y. Wang, C. Yu, L. Jiao, X. Wei, J. Fang, D. Xue and H. Yan, *ACS Appl. Mater. Interfaces*, 2022, **14**, 5470.
19 Y. Shi, W. Chen, Z. Wu, Y. Wang, W. Sun, K. Yang, Y. Tang, H. Y. Woo, M. Zhou, A. Djurisic, Z. He and X. Guo, *J. Mater. Chem. A*, 2020, **8**, 13754–13762.
20 W. Chen, Y. Shi, Y. Wang, X. Feng, A. B. Djurišić, H. Y. Woo, X. Guo and Z. He, *Nano Energy*, 2019, **68**, 104363.
21 A. A. Said, J. Xie and Q. Zhang, *Small*, 2019, **15**, 1900854.
22 J. Liu, Y. Shi, J. Dong, M. I. Nugraha, X. Qiu, M. Su, R. C. Chiechi, D. Baran, G. Portale, X. Guo and L. J. A. Koster, *ACS Energy Lett.*, 2019, **4**, 1556–1564.
23 Y. Shi, J. Li, H. Sun, Y. Li, Y. Wang, Z. Wu, S. Y. Jeong, H. Y. Woo, S. Fabiano and X. Guo, *Angew. Chem., Int. Ed.*, 2022, **61**, e202214192.
24 H. Guo, C.-Y. Yang, X. Zhang, A. Motta, K. Feng, Y. Xia, Y. Shi, Z. Wu, K. Yang, J. Chen, Q. Liao, Y. Tang, H. Sun, H. Y. Woo, S. Fabiano, A. Facchetti and X. Guo, *Nature*, 2021, **599**, 67–73.
25 Y. Lu, J.-Y. Wang and J. Pei, *Chem. Mater.*, 2019, **31**, 6412–6423.
26 Y. Lu, Z.-D. Yu, R.-Z. Zhang, Z.-F. Yao, H.-Y. You, L. Jiang, H.-I. Un, B.-W. Dong, M. Xiong, J.-Y. Wang and J. Pei, *Angew. Chem., Int. Ed.*, 2019, **58**, 11390–11394.
27 A. Tripathi, Y. Lee, S. Lee and H. Y. Woo, *J. Mater. Chem. C*, 2022, **10**, 6114–6140.
28 X. Yan, M. Xiong, J.-T. Li, S. Zhang, Z. Ahmad, Y. Lu, Z.-Y. Wang, Z.-F. Yao, J.-Y. Wang, X. Gu and T. Lei, *J. Am. Chem. Soc.*, 2019, **141**, 20215–20221.
29 M. Xiong, X. Yan, J.-T. Li, S. Zhang, Z. Cao, N. Prine, Y. Lu, J.-Y. Wang, X. Gu and T. Lei, *Angew. Chem., Int. Ed.*, 2021, **60**, 8189–8197.
30 B. Zhang, C. Ge, C. Xie, K. Lin, W. Yang, B. Liu, X. Gao, Y. Zhou and Q. Zhang, *J. Mater. Chem. C*, 2022, **10**, 17530–17538.
31 M. Comí, D. Patra, R. Yang, Z. Chen, A. Harbuzaru, Y. Wubulikasimu, S. Banerjee, R. Ponce Ortiz, Y. Liu and M. Al-Hashimi, *J. Mater. Chem. C*, 2021, **9**, 5113–5123.
32 Q. Che, W. Zhang, X. Wei, Y. Zhou, H. Luo, J. Wei, L. Wang and G. Yu, *CCS Chem.*, 2023, DOI: **10.31635/ccschem.023.202202458**.
33 Q. Liu, W. He, Y. Shi, S. Otep, W. L. Tan, S. Manzhos, C. R. McNeill, X. Guo, P. Sonar, T. Michinobu and A. K. K. Kyaw, *Chem. Mater.*, 2022, **34**, 3140–3151.
34 J. Yang, L. Zhao, Z. Yin, J. Wang, Y. Zhao, H. Chen and Y. Liu, *Macromolecules*, 2021, **54**, 3120–3129.
35 Y. Shi, H. Guo, M. Qin, J. Zhao, Y. Wang, H. Wang, Y. Wang, A. Facchetti, X. Lu and X. Guo, *Adv. Mater.*, 2018, **30**, 1705745.

36 Y. Shi, H. Guo, M. Qin, Y. Wang, J. Zhao, H. Sun, H. Wang, Y. Wang, X. Zhou, A. Facchetti, X. Lu, M. Zhou and X. Guo, *Chem. Mater.*, 2018, **30**, 7988–8001.
37 Y. Shi, W. Li, X. Wang, L. Tu, M. Li, Y. Zhao, Y. Wang and Y. Liu, *Chem. Mater.*, 2022, **34**, 1403–1413.
38 X. Guo, A. Facchetti and T. J. Marks, *Chem. Rev.*, 2014, **114**, 8943–9021.
39 Y. Wang, H. Guo, S. Ling, I. Arrechea-Marcos, Y. Wang, J. T. López Navarrete, R. P. Ortiz and X. Guo, *Angew. Chem., Int. Ed.*, 2017, **56**, 9924–9929.
40 Y. Wang, H. Guo, A. Harbuzaru, M. A. Uddin, I. Arrechea-Marcos, S. Ling, J. Yu, Y. Tang, H. Sun, J. T. López Navarrete, R. P. Ortiz, H. Y. Woo and X. Guo, *J. Am. Chem. Soc.*, 2018, **140**, 6095–6108.
41 C. Duan, J. Zhang, J. Xiang, X. Yang and X. Gao, *Angew. Chem., Int. Ed.*, 2022, **61**, e202201494.
42 H. Xin, B. Hou and X. Gao, *Acc. Chem. Res.*, 2021, **54**, 1737–1753.
43 T. Shen, W. Li, Y. Zhao, Y. Wang and Y. Liu, *Adv. Mater.*, 2023, **35**, 2210093.
44 Y. Sui, Y. Deng, T. Du, Y. Shi and Y. Geng, *Mater. Chem. Front.*, 2019, **3**, 1932–1951.
45 Y. Wang, E. Zeglio, H. Liao, J. Xu, F. Liu, Z. Li, I. P. Maria, D. Mawad, A. Herland, I. McCulloch and W. Yue, *Chem. Mater.*, 2019, **31**, 9797–9806.
46 T. Lei, J.-H. Dou, X.-Y. Cao, J.-Y. Wang and J. Pei, *J. Am. Chem. Soc.*, 2013, **135**, 12168–12171.
47 K. Feng, H. Guo, J. Wang, Y. Shi, Z. Wu, M. Su, X. Zhang, J. H. Son, H. Y. Woo and X. Guo, *J. Am. Chem. Soc.*, 2021, **143**, 1539–1552.
48 Y. Min, C. Dou, D. Liu, H. Dong and J. Liu, *J. Am. Chem. Soc.*, 2019, **141**, 17015–17021.
49 X. Shao, M. Liu, J. Liu and L. Wang, *Angew. Chem., Int. Ed.*, 2022, **61**, e202205893.
50 K. Zhao, Z.-F. Yao, Z.-Y. Wang, J.-C. Zeng, L. Ding, M. Xiong, J.-Y. Wang and J. Pei, *J. Am. Chem. Soc.*, 2022, **144**, 3091–3098.
51 J. Miao, Y. Wang, J. Liu and L. Wang, *Chem. Soc. Rev.*, 2021, **51**, 153–187.
52 R. Zhao, J. Liu and L. Wang, *Acc. Chem. Res.*, 2020, **53**, 1557–1567.
53 X. Guo and M. D. Watson, *Org. Lett.*, 2008, **10**, 5333–5336.
54 B. Liu, M. Böckmann, W. Jiang, N. L. Doltsinis and Z. Wang, *J. Am. Chem. Soc.*, 2020, **142**, 7092–7099.
55 W. Jiang, Y. Li and Z. Wang, *Acc. Chem. Res.*, 2014, **47**, 3135–3147.
56 Y. Wang, M. Nakano, T. Michinobu, Y. Kiyota, T. Mori and K. Takimiya, *Macromolecules*, 2017, **50**, 857–864.
57 Y. Wang and K. Takimiya, *Adv. Mater.*, 2020, **32**, 2002060.
58 H. Wang, Q. Shi, Y. Lin, H. Fan, P. Cheng, X. Zhan, Y. Li and D. Zhu, *Macromolecules*, 2011, **44**, 4213–4221.
59 M. Comí, M. U. Ocheje, S. Attar, A. U. Mu, B. K. Philips, A. J. Kalin, K. E. Kakosimos, L. Fang, S. Rondeau-Gagné and M. Al-Hashimi, *Macromolecules*, 2020, **54**, 665–672.
60 T. Hasegawa, M. Ashizawa, K. Aoyagi, H. Masunaga, T. Hikima and H. Matsumoto, *Org. Lett.*, 2017, **19**, 3275–3278.
61 Q. Shi, W.-Q. Chen, J. Xiang, X.-M. Duan and X. Zhan, *Macromolecules*, 2011, **44**, 3759–3765.
62 T. Hasegawa, M. Ashizawa, S. Kawauchi, H. Masunaga, N. Ohta and H. Matsumoto, *RSC Adv.*, 2019, **9**, 10807–10813.
63 Y. Wang and T. Michinobu, *J. Mater. Chem. C*, 2016, **4**, 6200–6214.
64 Y. Xie, T. Fujimoto, S. Dalgleish, Y. Shuku, M. M. Matsushita and K. Awaga, *J. Mater. Chem. C*, 2013, **1**, 3467.
65 F. A. Arroyave, C. A. Richard and J. R. Reynolds, *Org. Lett.*, 2012, **14**, 6138–6141.
66 Y. Wang, A. T. R. Tan, T. Mori and T. Michinobu, *J. Mater. Chem. C*, 2018, **6**, 3593–3603.
67 Y. H. Zhao, W. Li, T. Shen, Y. Zhao, Y. Liu and Y. Wang, *Sci. China: Chem.*, 2023, **66**, 548–561.